American Mineralogist, Volume 85, pages 1465–1473, 2000

In situ powder diffraction study of titanite ($CaTiOSiO_4$) at high pressure and high temperature

MARTIN KUNZ,[1,*] THILO ARLT,[2,†] AND JANO STOLZ[3]

[1]Labor für Kristallographie, ETH Zentrum, Sonneggstrasse 5, CH-8092 Zürich
[2]Bayerisches Geoinstitut, Universutät Bayreuth, D-95440 Bayreuth*
[3]Labor für mineralogische und chemische Kristallographie, Freiestrasse 3, CH-3012 Bern

ABSTRACT

A set of powder diffraction data was collected for synthetic titanite ($CaTiOSiO_4$) at simultaneously high pressures and high temperatures in a *P-T* field between 275 K to 650 K and room pressure to 4.9 GPa, respectively. With these data it was possible to relate the *A*2/*a* high-pressure phase at >3.5 GPa (room temperature) to the *A*2/*a* high temperature phase observed above 825 K (room pressure). The slope of the phase transition is –180 K/GPa. The data also allowed the extraction of *P-V-T* equations of state with the following parameters: for $P2_1/a$: $K_{298,0}$ = 113.4(3), $(\partial K_{T,0}/\partial T)_P$ = –0.061(3) GPa/K, $V_{298,0}$ = 369.04(2) Å^3, $\alpha_0 = 2.07(5)/10^5$ K. For *A*2/*a*: $K_{298,0}$ = 135.2(2), $(\partial K_{T,0}/\partial T)_P$ = –0.073(1) GPa/K, $V_{298,0}$ = 367.12(2) Å^3, $\alpha_0 = 2.8(2) / 10^5$ K, where *K* is bulk modulus, *V* is volume, and α is thermal expansivity. A structural analysis based on Rietveld refinements revealed that the polymerized CaO_7 polyhedra dominantly affect the structural response to changing pressure and temperature. The TiO_6 octahedra rotate almost rigidly in response to the compression of the CaO_7 polyhedra with which they share edges. The SiO_4 tetrahedra show a strong angular distortion with only little change in bond lengths.

INTRODUCTION

Titanite ($CaTiOSiO_4$), a rock forming mineral, is interesting for both geologists as well as material scientists. This not only because of its ability to retain radionucleids, which makes it a likely candidate as an inert host for nuclear waste disposal, but also for its interesting structural relation to the nonlinear optical material $KTiOPO_4$ (KTP). Both materials are structurally characterized by corner linked chains of TiO_6 octahedra. These chains are mutually connected via isolated tetrahedra, which are occupied by P^{5+} and Si^{4+} in KTP and titanite, respectively. Although the exact topology of the two compounds differ (e.g., Kunz et al. 1995), a common feature is the distinctive distortion of the TiO_6 units. This distortion, characterized by a shift of the central metal out of its otherwise regular oxygen octahedron, is caused by an electronic second-order Jahn-Teller effect and thus occurs around most octahedrally coordinated d^0 transition metals (Kunz and Brown 1994). This distortion induces a hyperpolarizability at the short titanyl bond that, if it is embedded in a non-centrosymmetric structure, gives rise to strong nonlinear optical effects. The crucial difference between KTP and titanite with respect to this distortion and to their physical properties is that in KTP all out-of-center distortions are oriented more or less parallel to each other, whereas in titanite these distortion-vectors are parallel within a TiO_6 chain, but correlate in an anti-ferroelectric way between adjacent chains (Fig. 1). This anti-ferroelectric interaction between adjacent TiO_6 chains in titanite cancels the locally induced hyper-polarizabilities and therefore inhibits any interesting nonlinear optical effects.

It is not yet clear what factors control the mutual interaction between the out-of-center distortions of neighboring chains. However, this interaction should be weak in titanite, as deduced from the disappearance of the correlation of distortion between adjacent TiO_6 chains at already moderate temperature (ca. 500 K). The loss of correlation is revealed by a phase transition with a change in space-group from $P2_1/a$ (ordered distortion vectors) to *A*2/*a* (disordered distortion vectors, e.g., Zhang et al. 1995). Hayward et al. (2000) show on the basis of heat capacity C_P, dielectric susceptibility and diffraction data (Bismayer et al. 1992; Zhang et al. 1995) that the excess entropy at the 500 K transition is very small (5.76 J/K-mol). Measurements of C_P (Tangeman and Xirouchakis 2000) confirm this low excess entropy at the 500 K transition. This low value is suspected to be connected to the smallness of the spontaneous strain associated with the dipole order-disorder phase-transition. This in turn is related to an unusually weak coupling between long-range order parameter (i.e., anti-ferroelectric coupling of dipoles) and strain. In addition, a small dilution of the concentration of out-of-center vectors by impurities, such as Al^{3+} or Fe^{3+} (observed in natural titanites, e.g., Oberti et al. 1991) or Sn^{4+} (Kunz et al. 1997), strongly affects this phase transition or even removes the stability field of the $P2_1/a$ phase.

Two additional phase changes exist, which mostly depend on the out-of-center distortion. The temperature induced isosymmetric ($A2/a \leftrightarrow A2/a$) transition around 825 K (Kek et

* E-mail: kunz@kristall.erdw.ethz.ch
† Present address: Grundlagenentwicklung Dauerwelle, Wella AG, D-64289 Darmstadt.

al. 1997) is interpreted as a change to a more symmetric Ti coordination based on softening of the Raman Ti-O stretching band. Another $P2_1/a \leftrightarrow A2/a$ phase transition is triggered by high pressure around 3.5 GPa (Kunz et al. 1996; Angel et al. 1999a). Based on crystal chemistry, this phase transition is assumed but not proven to be driven by a move of the Ti metal into the center of its coordination octahedron. To better understand the structural relationships between the pressure dependent phase transition and the two temperature driven phase changes, we collected powder diffraction data at simultaneously high pressure and temperature. This not only provides more structural information, but also yields further thermodynamic constraints on the intermediate phase between 500 K and 825 K.

Experimental methods

Synthetic titanite powder grown at subsolidus conditions (Xirouchakis et al. 1997) was loaded in a diamond anvil cell equipped with a resistance heater (Fei et al. 1992). The sample was embedded in a methanol/ethanol (4:1) pressure-transmitting medium together with NaCl, which served as a pressure marker. Data were collected along the *P-T* path shown in Figure 2 with a monochromatic [λ = 0.4859(2) Å] X-ray beam generated by two phased undulators of the ESRF beamline ID30 and selected with a channel cut Si-(111) monochromator. The powder diffraction patterns were recorded with a fast online image plate reader (Thoms et al. 1998). The 2D data were first corrected for flatfield effects and detector inherent distortions and then integrated into an intensity vs. 2-theta pattern using the procedure described by Hammersley et al. 1995, 1996, and Hammersley 1997. Final data analysis was done by Rietveld refinement using the program package GSAS (Larson and Von Dreele 1994). All profiles were first fitted with the Le Bail approach (Le Bail 1992) adjusting only cell-parameters and peak-profile coefficients. After convergence, these values were kept fixed for subsequent Rietveld refinement. For the Rietveld refinement, the U_{iso} for Ca, Ti, Si, and O were kept fixed at values of 0.008, 0.002, 0.0015, and 0.004 Å^2, respectively. For stable refinements a soft-constraint had to be applied to the Si-O bond-lengths. For refinements in space-group $P2_1/a$, we used a weighting factor of 10 and a target bond length of 1.63 Å. The weighting factor was reduced to 1.0 for refinements in space-group $A2/a$. For the final Rietveld refinement cycles, soft constraints were removed and cell parameters and peak profile coefficients were refined.

Results and discussion

The results of the Rietveld refinements are summarized on Table 1.

$P2_1/a \leftrightarrow A2/a$ Phase Transition

The location of the $P2_1/a \leftrightarrow A2/a$ phase transition in titanite is not straightforward with powder diffraction. It can most reliably be done based on the presence of $k + l$ = odd reflections, which are allowed in $P2_1/a$ but forbidden in $A2/a$. However, most of the strong $k + l$ = odd reflections overlap with other reflections which are not space-group sensitive and can thus not be used in a powder pattern. The only well-resolved reflections of the $k + l$ = odd class are the $22\bar{1}$ and $21\bar{2}$ (Kunz et al. 1996) which we used to monitor the phase transition on the basis of their presence in the powder pattern. This revealed that the $P2_1/a \leftrightarrow A2/a$ phase transition has a negative slope of about –180 K/GPa (Fig. 2). The phase boundary extrapolates to around 3.5 GPa at room temperature, consistent with previous experiments at 300 K (Angel et al. 1999a; Kunz et al. 1996). Extrapolating the phase boundary linearly to ambient pressure yields a temperature of about 880 K (Fig. 2). This suggests, that the high-pressure $A2/a$ phase corresponds to the high-symmetry phase above 825 K rather than to the disordered inter-

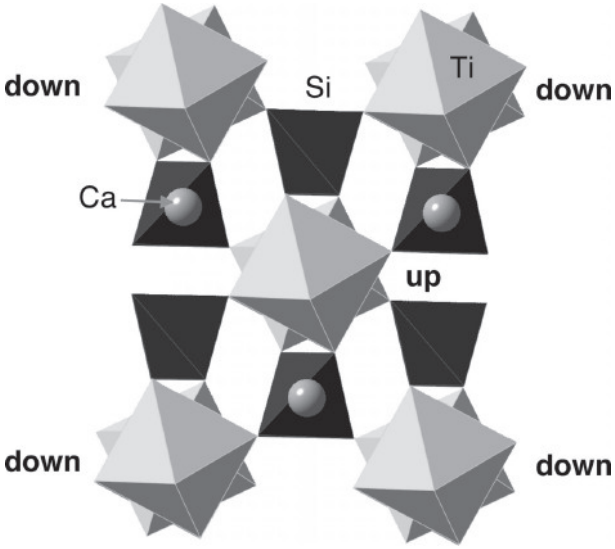

Figure 1. Polyhedral model of the titanite structure projected parallel *a*, i.e., parallel to the chains of TiO_6-octahedra. The labels "up" and "down" denote the direction of the out-of-center distortion with respect to the projection plane.

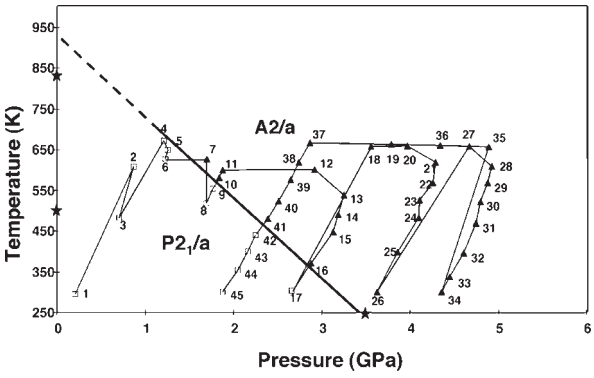

Figure 2. Pressure-temperature path for the powder diffraction experiments in the diamond anvil cell. Solid triangles represent data sets refined in space group $A2/a$; open squares stand for patterns, which were refined in space group $P2_1/a$. The solid line is indicating the approximate position of the $P21/a \leftrightarrow A2/a$ phase boundary. Its linear extrapolation (dashed) to room-pressure suggests the 825 K phase to be identical with the high-pressure phase. The stars indicate the location of the high-pressure and high-temperature phase transitions, respectively.

mediate *A*2/*a* phase between 496 K and 825 K. This result confirms the crystal chemical interpretation of the high-pressure structure as a structure characterized by a truly symmetric Ti-coordination rather than by a disorder of the out-of-center distortion vector (Kunz et al. 1996).

Chrosch et al. (1997), Zhang et al. (1995) and Bismayer et al. (1992) investigated the intensity variation of the super-lattice reflection as a function of temperature in the $P2_1/a$ phase. They show that below 500 K, the intensity decreases in a non-linear way to zero at the critical temperature (T_c). They model the variation of the intensity as $I \propto Q^2 \propto Q_0^2|T - T_c|^{2\beta}$, with a transition temperature T_c of 495.6 K and a critical exponent β of 0.14(1). Angel et al. (1999a) found that for the phase transition at high pressure, the intensities of the super-lattice reflections, and thus the square of the order parameter (Q) vary linearly with pressure, suggesting that pressure may suppress non-linearity of the variation of Q^2. This hypothesis holds for our case: the normalized intensity of $22\bar{1}$ and $21\bar{2}$ shows a (within experimental uncertainty) linear variation with both, $|T - T_c|$ and $|P - P_c|$. Pressure thus seems to suppress not only the pressure-dependent but also the temperature dependent non-linearity of Q^2-variation. Volume strain can be used to test this hypothesis. The volume-strain ($V_s = V'_{(A2/a)}/V - 1$) transforms according to the A_g representation and is thus proportional to Q^2, which is confirmed by our data within the limits of the uncertainty of the relatively weak super-lattice reflections. To better investigate the true nature of the phase-change in *P-T*-space, we plan for more accurate single crystal diffraction data.

The question remains how the intermediate *A*2/*a* phase reacts on pressure. Accurate single-crystal data between 465 K and 850 K in a very narrow and low-pressure regime are needed to answer this question.

COMPRESSIBILITY

Among the 45 *P-V-T* data points, 13 were collected in the $P2_1/a$ stability field whereas the remaining 32 were refined in space group *A*2/*a*. Data were collected by changing temperature at a given pressure, because the metal in the DAC gaskets only allows limited pressure cycling. It also minimizes deviatoric stress on the sample due to the annealing effect of high temperature. The disadvantage, however, is that it creates mainly isochoric data and thus only few isothermal and no isobaric data series. We therefore could not determine isothermal bulk moduli or isobaric thermal expansion values directly. Instead we used the full data subsets to fit a *P-V-T* third-order Birch-Murnaghan equation of state (Birch 1947).

$$P = \frac{3}{2} K_{T,0} \left[\left(\frac{V_{T,0}}{V} \right)^{\frac{7}{3}} - \left(\frac{V_{T,0}}{V} \right)^{\frac{5}{3}} \right] \left\{ 1 - \frac{3}{4} \left(4 - K'_{T,0} \right) \left[\left(\frac{V_{T,0}}{V} \right)^{\frac{2}{3}} - 1 \right] \right\} \quad (1)$$

This procedure has been proposed by Saxena and Zhang (1990) and Martinez et al. (1997) and is derived in detail in Fiquet et al. (1998). It is based on substitution of $K_{T,0}$ by a function of $K_{298,0}$ and $\partial K_{T,0}/\partial T$, and $V_{T,0}$ by a function of $V_{298,0}$, α_0, and α_1 into Equation 1. This leaves us with $V_{298,0}$, $K_{298,0}$, $\partial K/\partial P_{298,0}$, $\partial K_{T,0}/\partial T$, α_0, and α_1 as refineable parameters. Due to the limited *P-T* spread of our two subsets we decided to fix $\partial K/\partial P$ and α_1 to values of 4 and 0, respectively, to achieve stable convergence. For the fit, data were weighted with the inverse of the pressure uncertainty, which was estimated as

$$\sigma_P^2 = \sigma_P^2 + \sigma_V^2 \left(\frac{K}{V} \right)^2 + \sigma_T^2 (\alpha K)^2 \quad (2)$$

where σ_P is the total estimated pressure uncertainty, σ_p. the uncertainty from the pressure measurement, σ_V the volume uncertainty of the pressure standard and σ_T, the temperature uncertainty (Angel 2000).

With this procedure, and by using the room temperature data of Angel et al. (1999a, 1999b) to better constrain $K_{298,0}$ we obtained the following thermoelastic parameters for $P2_1/a$- and *A*2/*a* (high-symmetry) titanite:

$$P2_1/a\text{: } K_{298,0} = 113.4(3),\ \left(\frac{\partial K_{T,0}}{\partial T} \right)_P = -0.061(3)\ \text{GPa/K},\ V_{298,0} = 369.04(2)\ \text{Å}^3,\ \alpha_0 = 2.07(5) / 10^5\ \text{K}. \quad (3)$$

$$A2/a\text{: } K_{298,0} = 135.2(2),\ \left(\frac{\partial K_{T,0}}{\partial T} \right)_P = -0.073(1)\ \text{GPa/K},\ V_{298,0} = 367.12(2)\ \text{Å}^3,\ \alpha_0 = 2.8(2) / 10^5\ \text{K}. \quad (4)$$

One should keep in mind, however, that the standard deviations indicated are analytical and do not represent the uncertainty of the assumptions for K' and α_1. Various fits with different combinations of K' and α_1 between 4 and 6 (K') and 0 and $6 \cdot 10^{-8}$ (α_1) can give a feeling of the true uncertainties: Increasing K' to 6 leads to a reduction of K_0 by about 10 GPa. Increasing α_1 to $6 \cdot 10^{-8}$ leads to a reduction of α_0 to very low (10^{-6}) and even negative values. It should be also mentioned here, that the high values for the temperature dependence of K_0 may be an indication for elastic softening around the phase transition (Carpenter and Salje 1998). This of course would make the use of a conventional equation of state for any phase above or below the phase transition invalid.

The lack of isobaric and isothermal data makes it difficult to directly compare the reverse effects of pressure and temperature on the individual cell parameters. From the pseudo-isochoric series (e.g., 37 to 45; 28 to 34), we however can estimate that a temperature change of –350 K has roughly the same effect on the volume as a pressure change of 1 GPa. We can also look at the change of the cell parameters as a function of cell volume and compare this with the behavior at high temperature or high pressure only. Here we find that the thermoelastic behavior of titanite is somewhat unusual: unlike most compounds titanite does not show an inverse relationship between the orientation of the elastic tensor and the orientation of the thermal expansion tensor. From data collected at high pressure (Kunz et al. 1997; Angel et al. 1999a, 1999b) or high temperature (Taylor and Brown 1976; Kek et al. 1997), the b axis is the stiffest on compression but is also the one showing the largest thermal expansion. If we plot the relative cell axes vs. the volume of our *P-V-T* data (Fig. 3), we find that for the *P-T* spread of our data set, the change in volume is clearly dominated by the pressure effect, because it shows the same characteristics as is observed for *P-V*-data, i.e., a smaller change in b

TABLE 1. Cell parameters and fractional coordinates for the individual *P-T*-points as derived from Rietveld refinement

P-T-Point*	001	002	003	004	005	006	007	008	009
Pressure (GPa)	0.21	0.87	0.71	1.21	1.26	1.23	1.70	1.69	1.77
Temperature (K)	300	609	483	670	648	628	627	518	555
Space Group	$P2_1/a$	$P2_1/a$	$P2_1/a$	$P2_1/a$	$P2_1/a$	$P2_1/a$	$A2/a$	$P2_1/a$	$P2_1/a$
a (Å)	7.0572(3)	7.0512(4)	7.0494(3)	7.0442(3)	7.0391(3)	7.0411(3)	7.0246(4)	7.0187(4)	7.0186(3)
b (Å)	8.7108(4)	8.7141(5)	8.7102(5)	8.7132(5)	8.7100(4)	8.7106(4)	8.7037(6)	8.6965(5)	8.6983(4)
c (Å)	6.5534(4)	6.5521(4)	6.5484(4)	6.5476(4)	6.5433(3)	6.5441(3)	6.5329(5)	6.5243(4)	6.5272(4)
β (°)	113.786(5)	113.735(6)	113.742(5)	113.705(5)	113.686(5)	113.682(5)	113.619(7)	113.594(6)	113.617(5)
Ca(x)	0.239(4)	0.244(4)	0.255(6)	0.264(6)	0.264(3)	0.265(4)	¼	0.266(6)	0.274(6)
Ca(y)	0.913(1)	0.924(4)	0.919(2)	0.914(2)	0.913(1)	0.915(1)	0.1608(17)	0.912(2)	0.911(2)
Ca(z)	0.750(5)	0.744(8)	0.757(10)	0.743(8)	0.738(5)	0.739(5)	0	0.754(8)	0.766(8)
Ti(x)	0.527(3)	0.503(6)	0.499(5)	0.517(5)	0.525(3)	0.512(5)	½	0.525(5)	0.519(5)
Ti(y)	0.753(3)	0.747(7)	0.748(5)	0.751(4)	0.748(3)	0.746(3)	0	0.756(5)	0.755(7)
Ti(z)	0.246(3)	0.241(7)	0.256(6)	0.243(5)	0.246(4)	0.244(5)	½	0.254(6)	0.254(8)
Si(x)	0.759(4)	0.738(10)	0.735(7)	0.736(8)	0.726(5)	0.728(5)	¾	0.753(9)	0.755(11)
Si(y)	0.934(2)	0.923(3)	0.929(2)	0.932(2)	0.936(2)	0.935(2)	0.182(2)	0.931(2)	0.934(3)
Si(z)	0.774(4)	0.756(9)	0.752(10)	0.757(9)	0.752(7)	0.756(7)	0	0.745(9)	0.748(13)
O1(x)	0.766(10)	0.871(6)	0.755(6)	0.784(12)	0.750(11)	0.736(13)	¾	0.808(9)	0.869(7)
O1(y)	0.810(2)	0.780(7)	0.806(5)	0.814(3)	0.829(3)	0.818(3)	0.073(3)	0.813(3)	0.788(6)
O1(z)	0.270(9)	0.251(8)	0.251(7)	0.235(14)	0.249(15)	0.249(15)	½	0.241(1)	0.247(10)
O2(x)	0.897(5)	0.926(11)	0.920(9)	0.907(9)	0.899(7)	0.902(8)		0.916(8)	0.912(11)
O2(y)	0.800(4)	0.816(10)	0.817(9)	0.807(9)	0.813(5)	0.813(7)		0.813(8)	0.811(11)
O2(z)	0.928(5)	0.932(15)	0.923(11)	0.933(10)	0.923(7)	0.918(8)		0.934(12)	0.940(15)
O3(x)	0.353(6)	0.378(12)	0.386(10)	0.367(12)	0.369(8)	0.367(8)	0.894(3)	0.392(9)	0.403(12)
O3(y)	0.945(5)	0.955(9)	0.947(7)	0.950(7)	0.949(5)	0.944(6)	0.064(3)	0.968(9)	0.971(13)
O3(z)	0.125(6)	0.142(14)	0.162(14)	0.139(14)	0.126(9)	0.124(9)	0.195(3)	0.176(13)	0.176(18)
O4(x)	0.895(5)	0.930(12)	0.918(9)	0.922(9)	0.929(6)	0.920(8)		0.910(8)	0.942(12)
O4(y)	0.338(4)	0.310(10)	0.308(9)	0.319(8)	0.319(6)	0.316(7)		0.319(9)	0.319(11)
O4(z)	0.436(5)	0.433(15)	0.438(11)	0.452(10)	0.452(7)	0.442(8)		0.453(12)	0.432(15)
O5(x)	0.378(5)	0.389(12)	0.370(11)	0.371(10)	0.368(6)	0.373(7)	0.376(3)	0.369(9)	0.387(14)
O5(y)	0.468(4)	0.466(9)	0.468(7)	0.461(7)	0.454(5)	0.462(5)	0.211(3)	0.454(9)	0.458(13)
O5(z)	0.646(7)	0.682(15)	0.656(14)	0.674(13)	0.678(8)	0.672(9)	0.402(3)	0.649(12)	0.655(18)
R(p) (%)	0.89	1.70	1.48	1.74	1.41	1.26	1.85	1.52	1.83
R(wp) (%)	1.59	2.68	2.35	2.61	2.23	2.06	2.78	2.35	2.12
$R(F^2)$ (%)	4.43	17.5	16.83	16.7	13.89	13.92	18.5	13.64	15.9

* Run numbers are HS349-XXX.

TABLE 1—*Continued*

P-T-Point HS349_xxx	019	020	021	022	023	024	025	026	027
Pressure (GPa)	3.97	4.29	4.26	4.11	4.10	3.86	3.63	4.67	4.93
Temperature (K)	659	618	568	525	483	399	301	658	609
Space Group	$A2/a$	$A2/a$	$A2/a$	$A2/a$	$A2/a$	$A2/a$	$A2/a$	$A2/a$	$A2/a$
a (Å)	6.9656(4)	6.9560(5)	6.9529(5)	6.9540(5)	6.9527(5)	6.9543(6)	6.9559(6)	6.9496(5)	6.9413(6)
b (Å)	8.6709(5)	8.6644(7)	8.6610(7)	8.6603(7)	8.6576(6)	8.6586(8)	8.6586(8)	8.6605(7)	8.6549(8)
c (Å)	6.4816(4)	6.4713(6)	6.4677(7)	6.4674(6)	6.4666(6)	6.4707(8)	6.4672(6)	6.4654(6)	6.4570(8)
β (°)	113.399(7)	113.358(9)	113.347(10)	113.348(9)	113.349(10)	113.380(1)	113.376(1)	113.342(10)	113.317(12)
Ca(x)	¼	¼	¼	¼	¼	¼	¼	¼	¼
Ca(y)	0.166(1)	0.166(1)	0.166(1)	0.163(1)	0.165(1)	0.161(2)	0.165(2)	0.165(2)	0.164(2)
Ca(z)	0	0	0	0	0	0	0	0	0
Ti(x)	½	½	½	½	½	½	½	½	½
Ti(y)	0	0	0	0	0	0	0	0	0
Ti(z)	½	½	½	½	½	½	½	½	½
Si(x)	¾	¾	¾	¾	¾	¾	¾	¾	¾
Si(y)	0.193(2)	0.195(2)	0.196(2)	0.197(2)	0.188(2)	0.196(3)	0.196(2)	0.194(3)	0.194(3)
Si(z)	0	0	0	0	0	0	0	0	0
O1(x)	¾	¾	¾	¾	¾	¾	¾	¾	¾
O1(y)	0.052(3)	0.053(3)	0.057(3)	0.048(3)	0.043(3)	0.032(4)	0.047(4)	0.057(3)	0.051(4)
O1(z)	½	½	½	½	½	½	½	½	½
O2(x)									
O2(y)									
O2(z)									
O3(x)	0.930(2)	0.926(3)	0.921(3)	0.924(6)	0.923(3)	0.928(3)	0.925(3)	0.923(3)	0.923(3)
O3(y)	0.069(2)	0.070(2)	0.069(2)	0.071(2)	0.072(2)	0.076(2)	0.071(2)	0.071(2)	0.074(2)
O3(z)	0.176(2)	0.174(3)	0.170(3)	0.172(3)	0.179(3)	0.177(4)	0.169(3)	0.176(3)	0.178(4)
O4(x)									
O4(y)									
O4(z)									
O5(x)	0.398(2)	0.396(3)	0.398(3)	0.396(3)	0.396(3)	0.393(3)	0.398(3)	0.394(3)	0.397(3)
O5(y)	0.219(2)	0.219(2)	0.214(2)	0.217(2)	0.219(2)	0.215(2)	0.217(2)	0.219(2)	0.221(3)
O5(z)	0.390(3)	0.387(3)	0.392(4)	0.388(3)	0.394(3)	0.387(4)	0.394(4)	0.383(4)	0.386(4)
R(p) (%)	1.36	1.51	1.52	1.56	1.59	1.92	1.68	1.58	1.65
R(wp) (%)	2.42	2.63	2.59	2.58	2.58	2.96	2.83	2.75	2.89
$R(F^2)$ (%)	8.38	8.92	8.03	8.76	8.48	7.60	8.70	8.76	7.60

TABLE 1—*Extended*

P-T-Point HS349_xxx	010	011	012	013	014	015	016	017	018
Pressure (GPa)	1.84	1.88	2.87	3.25	3.19	3.13	2.88	2.66	3.56
Temperature (K)	581	560	666	538	490	448	371	303	658
Space Group	*A*2/*a*	*A*2/*a*	*A*2/*a*	*A*2/*a*	*A*2/*a*	*A*2/*a*	*A*2/*a*	$P2_1/a$	*A*2/*a*
a (Å)	7.0169(3)	7.0158(3)	6.9915(2)	6.9754(5)	6.9749(5)	6.9736(5)	6.9786(4)	6.9820(4)	6.9737(4)
b (Å)	8.6981(5)	8.6986(5)	8.6881(3)	8.6723(7)	8.6726(7)	8.6716(7)	8.6726(6)	8.6748(5)	8.6760(5)
c (Å)	6.5264(5)	6.5257(4)	6.5068(3)	6.4885(6)	6.4885(6)	6.4889(6)	6.4910(5)	6.4924(4)	6.4902(4)
β (°)	113.603(5)	113.592(6)	113.492(4)	113.443(10)	113.466(9)	113.487(9)	113.491(7)	113.498(7)	113.434(7)
Ca(x)	¼	¼	¼	¼	¼	¼	¼	0.253(5)	¼
Ca(y)	0.159(1)	0.159(1)	0.163(1)	0.164(2)	0.162(1)	0.162(1)	0.165(1)	0.916(1)	0.168(1)
Ca(z)	0	0	0	0	0	0	0	0.744(5)	0
Ti(x)	½	½	½	½	½	½	½	0.493(4)	½
Ti(y)	0	0	0	0	0	0	0	0.732(2)	0
Ti(z)	½	½	½	½	½	½	½	0.246(5)	½
Si(x)	¾	¾	¾	¾	¾	¾	¾	0.712(4)	¾
Si(y)	0.188(2)	0.188(2)	0.193(2)	0.196(2)	0.195(2)	0.195(2)	0.188(2)	0.935(2)	0.191(2)
Si(z)	0	0	0	0	0	0	0	0.752(5)	0
O1(x)	¾	¾	¾	¾	¾	¾	¾	0.727(10)	¾
O1(y)	0.075(2)	0.079(3)	0.063(3)	0.063(4)	0.050(3)	0.048(3)	0.051(3)	0.802(3)	0.058(3)
O1(z)	½	½	½	½	½	½	½	0.242(12)	½
O2(x)								0.901(5)	
O2(y)								0.816(5)	
O2(z)								0.921(6)	
O3(x)	0.912(2)	0.915(2)	0.916(3)	0.919(3)	0.925(2)	0.929(2)	0.924(2)	0.419(7)	0.926(2)
O3(y)	0.069(2)	0.069(2)	0.067(2)	0.072(2)	0.067(2)	0.068(2)	0.067(2)	0.950(4)	0.067(2)
O3(z)	0.186(2)	0.187(2)	0.175(3)	0.176(3)	0.173(3)	0.176(3)	0.180(3)	0.146(7)	0.175(2)
O4(x)								0.952(5)	
O4(y)								0.308(5)	
O4(z)								0.434(7)	
O5(x)	0.380(2)	0.384(3)	0.401(3)	0.405(3)	0.404(3)	0.402(3)	0.391(3)	0.376(6)	0.395(2)
O5(y)	0.213(2)	0.213(2)	0.220(2)	0.225(3)	0.220(2)	0.214(2)	0.214(2)	0.477(4)	0.216(2)
O5(z)	0.395(3)	0.401(3)	0.402(3)	0.396(4)	0.401(3)	0.395(3)	0.394(3)	0.670(8)	0.397(3)
R(p) (%)	1.33	1.41	0.93	1.47	1.46	1.64	1.38	1.34	1.32
R(wp) (%)	2.16	2.26	1.63	2.30	2.31	2.68	2.35	2.24	2.32
$R(F^2)$ (%)	9.8	9.84	6.82	8.76	7.20	7.74	6.92	8.68	7.58

P-T-Point HS349_xxx	028	029	030	031	032	033	034	035	036
Pressure (GPa)	4.88	4.80	4.75	4.61	4.45	4.36	4.89	4.34	3.79
Temperature (K)	568	522	469	396	338	301	656	660	662
Space-Group	*A*2/*a*	*A*2/*a*	*A*2/*a*	*A*2/*a*	*A*2/*a*	*A*2/*a*	*A*2/*a*	*A*2/*a*	*A*2/*a*
a (Å)	6.9410(5)	6.9409(5)	6.9395(6)	6.9385(6)	6.9399(7)	6.9414(6)	6.9443(5)	6.9534(4)	6.9664(3)
b (Å)	8.6539(7)	8.6532(8)	8.6529(9)	8.6498(9)	8.6524(10)	8.6521(8)	8.6582(7)	8.6641(7)	8.6728(5)
c (Å)	6.4559(7)	6.4551(7)	6.4550(8)	6.4533(8)	6.4547(9)	6.4553(7)	6.4621(6)	6.4730(5)	6.4846(4)
β (°)	113.333(10)	113.331(11)	113.338(12)	113.348(13)	113.352(14)	113.357(11)	113.327(10)	113.361(8)	113.400(6)
Ca(x)	¼	¼	¼	¼	¼	¼	¼	¼	¼
Ca(y)	0.161(1)	0.160(1)	0.161(2)	0.160(2)	0.161(2)	0.162(1)	0.164(1)	0.165(1)	0.167(1)
Ca(z)	0	0	0	0	0	0	0	0	0
Ti(x)	½	½	½	½	½	½	½	½	½
Ti(y)	0	0	0	0	0	0	0	0	0
Ti(z)	½	½	½	½	½	½	½	½	½
Si(x)	¾	¾	¾	¾	¾	¾	¾	¾	¾
Si(y)	0.193(2)	0.194(3)	0.195(3)	0.196(3)	0.198(3)	0.196(2)	0.192(2)	0.194(2)	0.195(2)
Si(z)	0	0	0	0	0	0	0	0	0
O1(x)	¾	¾	¾	¾	¾	¾	¾	¾	¾
O1(y)	0.049(3)	0.049(3)	0.048(4)	0.042(4)	0.047(4)	0.045(4)	0.056(3)	0.057(3)	0.059(3)
O1(z)	½	½	½	½	½	½	½	½	½
O2(x)									
O2(y)									
O2(z)									
O3(x)	0.923(3)	0.920(3)	0.922(3)	0.919(3)	0.922(3)	0.923(3)	0.919(3)	0.917(3)	0.915(2)
O3(y)	0.073(2)	0.073(2)	0.075(2)	0.077(2)	0.077(3)	0.076(2)	0.069(2)	0.068(2)	0.066(2)
O3(z)	0.176(3)	0.177(3)	0.175(3)	0.177(4)	0.172(4)	0.174(3)	0.178(3)	0.171(3)	0.167(2)
O4(x)									
O4(y)									
O4(z)									
O5(x)	0.386(3)	0.388(3)	0.392(3)	0.389(3)	0.392(4)	0.393(3)	0.394(3)	0.391(3)	0.390(2)
O5(y)	0.217(2)	0.216(2)	0.219(2)	0.218(2)	0.219(3)	0.221(2)	0.218(2)	0.211(2)	0.210(2)
O5(z)	0.380(3)	0.381(3)	0.383(4)	0.378(4)	0.381(4)	0.383(3)	0.388(3)	0.389(3)	0.390(3)
R(p) (%)	1.43	1.49	1.84	1.66	1.73	1.62	1.46	1.30	1.08
R(wp) (%)	2.42	2.55	3.13	2.80	3.02	2.82	2.65	2.44	1.94
$R(F^2)$ (%)	6.41	5.84	6.47	5.97	6.11	6.71	7.93	7.84	7.33

—*Continued next page.*

TABLE 1—*Continued*

P-T-Point HS349_xxx	037	038	039	040	041	042	043	044	045
Pressure (GPa)	2.87	2.74	2.65	2.51	2.39	2.25	2.16	2.05	1.88
Temperature (K)	666	619	576	523	481	440	399	354	301
Space Group	*A2/a*	*A2/a*	*A2/a*	*A2/a*	*A2/a*	$P2_1/a$	$P2_1/a$	$P2_1/a$	$P2_1/a$
a (Å)	6.9915(2)	6.9926(3)	6.9915(3)	6.9929(3)	6.9950(3)	6.9982(2)	6.9990(3)	6.9984(3)	7.0014(3)
b (Å)	8.6881(3)	8.6872(4)	8.6849(4)	8.6850(4)	8.6858(4)	8.6853(3)	8.6860(4)	8.6846(4)	8.6869(4)
c (Å)	6.5068(3)	6.5068(3)	6.5051(3)	6.5059(3)	6.5068(3)	6.5079(3)	6.5073(3)	6.5063(3)	6.5081(3)
β (°)	113.492(4)	113.494(5)	113.497(5)	113.508(5)	113.516(5)	113.523(4)	113.521(4)	113.521(4)	113.533(4)
Ca(x)	¼	¼	¼	¼	¼	0.257(3)	0.254(3)	0.255(3)	0.256(3)
Ca(y)	0.1674(9)	0.168(1)	0.168(1)	0.168(1)	0.168(1)	0.917(8)	0.9172(9)	0.917(1)	0.9159(9)
Ca(z)	0	0	0	0	0	0.762(4)	0.759(4)	0.759(4)	0.762(4)
Ti(x)	½	½	½	½	½	0.524(2)	0.524(2)	0.526(3)	0.526(2)
Ti(y)	0	0	0	0	0	0.753(2)	0.757(2)	0.759(2)	0.757(2)
Ti(z)	½	½	½	½	½	0.238(3)	0.235(3)	0.236(3)	0.237(2)
Si(x)	¾	¾	¾	¾	¾	0.727(3)	0.727(4)	0.724(4)	0.723(3)
Si(y)	0.189(1)	0.191(2)	0.190(2)	0.190(2)	0.190(2)	0.936(1)	0.938(2)	0.936(2)	0.937(2)
Si(z)	0	0	0	0	0	0.758(4)	0.758(5)	0.758(5)	0.755(5)
O1(x)	¾	¾	¾	¾	¾	0.783(6)	0.783(7)	0.782(7)	0.779(7)
O1(y)	0.050(2)	0.059(2)	0.058(2)	0.060(2)	0.063(3)	0.807(2)	0.817(2)	0.820(2)	0.822(2)
O1(z)	½	½	½	½	½	0.275(6)	0.277(7)	0.274(8)	0.275(7)
O2(x)						0.913(4)	0.909(5)	0.911(5)	0.910(4)
O2(y)						0.819(3)	0.815(4)	0.816(4)	0.817(4)
O2(z)						0.912(4)	0.909(5)	0.910(5)	0.909(5)
O3(x)	0.908(2)	0.907(2)	0.907(2)	0.907(2)	0.908(2)	0.394(5)	0.385(6)	0.382(6)	0.377(6)
O3(y)	0.066(1)	0.066(1)	0.065(2)	0.065(2)	0.065(2)	0.948(3)	0.936(4)	0.934(4)	0.931(3)
O3(z)	0.175(2)	0.174(2)	0.174(2)	0.174(2)	0.174(2)	0.138(6)	0.138(7)	0.137(7)	0.134(6)
O4(x)						0.912(4)	0.911(5)	0.912(5)	0.912(4)
O4(y)						0.320(4)	0.317(4)	0.316(4)	0.315(4)
O4(z)						0.445(4)	0.446(5)	0.447(4)	0.448(4)
O5(x)	0.386(2)	0.383(2)	0.381(2)	0.380(2)	0.379(2)	0.367(5)	0.369(6)	0.372(5)	0.374(5)
O5(y)	0.210(1)	0.206(2)	0.206(2)	0.207(2)	0.206(2)	0.473(3)	0.470(3)	0.472(3)	0.469(3)
O5(z)	0.398(2)	0.398(2)	0.396(2)	0.395(2)	0.393(2)	0.648(6)	0.650(7)	0.656(7)	0.659(6)
R(p) (%)	0.93	1.07	1.15	1.12	1.10	0.98	1.07	1.04	1.06
R(wp) (%)	1.63	1.92	2.12	2.05	2.01	1.69	1.89	1.87	1.87
$R(F^2)$ (%)	6.82	7.64	8.04	7.77	7.85	8.23	9.58	8.4	8.51

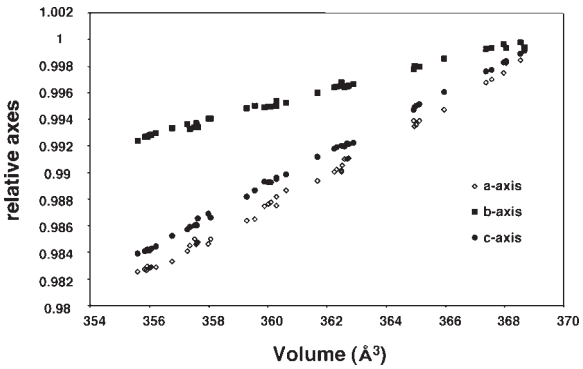

FIGURE 3. Evolution of relative axis-lengths as a function of volume. Note the significantly stiffer behavior of the *b* axis compared to *a* and *c*. Most of the scatter is due to the combined *P-T* data, indicating a slightly different dependence of the axes on a volume change due to pressure and temperature respectively.

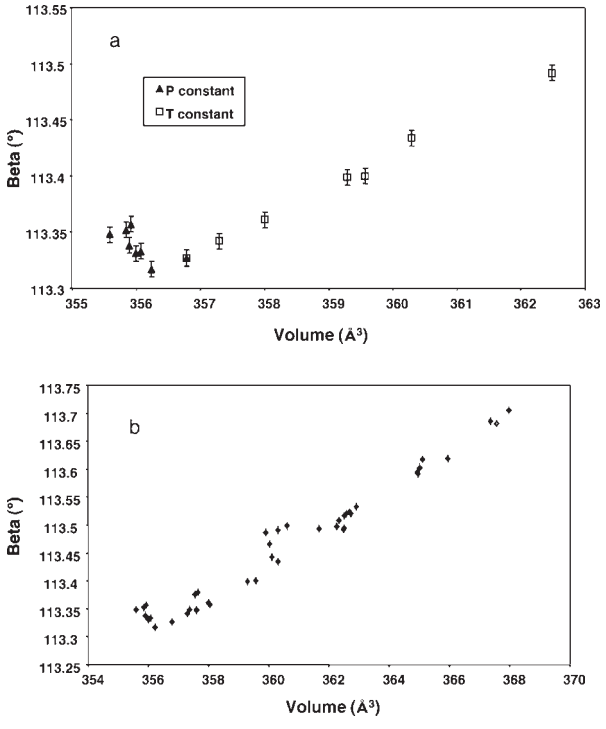

FIGURE 4. (**a**) Change of the monoclinic angle β with volume for some selected *A2/a* data at constant pressure (solid triangles) and constant temperature (open squares) respectively. Note the inverse behavior of β depending whether a volume change is due to changing pressure or changing temperature. The constant pressure data range between 300 and 600 K; the constant temperature data are between 2.9 and 4.9 GPa. (**b**) Variation of β with changing volume. The values are spread over a band due to the opposite effects of pressure and temperature, respectively. The overall positive correlation is due to the pressure changes. The scatter around this line is due to changing temperature.

for a given volume change than for a and c.

Even more peculiar is the behavior of the monoclinic angle β, which shows a decrease with decreasing volume upon compression, but an increase with decreasing volume due to cooling. For some pseudo-isobaric and isothermal *A2/a* data (Fig. 4a), the effect on β is much stronger for a pressure change of 2 GPa compared to a temperature change of 350 K. This is also reflected if we compare β and the volume of the full *A*2/*a* data set (Fig. 4b). The evolution of the monoclinic angle with changing volume is clearly dominated by the changing pressure. Changes in temperature merely cause the scatter around a straight β vs. V-line. This behavior cannot be explained by a domination of the spontaneous strain on the unit-cell behavior. This could only hold for the $P2_1/a$-phase, whereas our observation applies also for the *A2/a* phase. The opposite behavior of the titanite β-angle with changing pressure and temperature, respectively, suggests that high-pressure data cannot always be predicted by low temperature experiments.

STRUCTURAL EVOLUTION

The structural topology response to the externally imposed volume change is of interest. Most of the volume change across the pressure induced phase transition is accommodated by changes in the Ca-O bond length (Kunz et al. 1996). This behavior is also reflected in our *P-V-T* data set for general changes of volume (Fig. 5a) within the *A*2/*a* phase only. Standard deviations for bond lengths from Rietveld refinements of HT/HP data are quite high (~0.02 Å). Hence, a positive correlation is evident between volume and average <Ca-O> bonds, but cannot be resolved for the <Ti-O> and <Si-O> (Fig. 5b) bonds. There might be a slight negative correlation between <Si-O> bonds and volume. However, this has to be interpreted with caution, because soft constraints were applied to the Si-O bonds during the initial stages of the Rietveld refinement. Nevertheless, a closer look shows that this weak correlation could be real. For this, it is useful to first investigate another counterintuitive trend: as did Kunz et al. (1996) we observe the seemingly paradox trend of an opening of the Ti-O1-Ti angle (Fig. 7) with decreasing volume (Fig. 6a). This implies a straightening and thus extension of the corner-linked octahedral chain. It also implies a significant rigid body rotation of the Ti-octahedra, because the O3-Ti-O1 angle (Fig. 7) does not vary significantly as a function of volume change (Fig. 6a). Also, the distance between two unconnected neighboring octahedral corners (O3 in *A*2/*a* structures; Fig. 7) decreases with increasing volume (Fig. 6b), in accord with a rigid straightening of the octahedral chain. As shown by calculations of the phonon-density of states as a function of frequency (Hammonds et al. 1998),

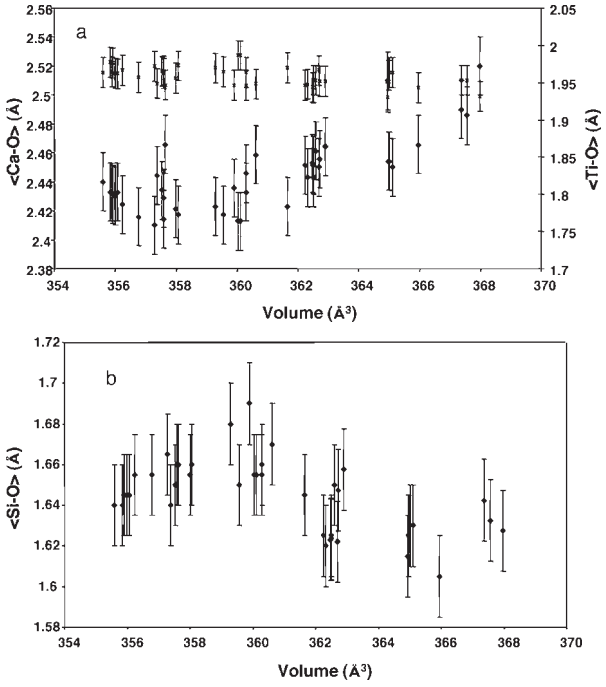

FIGURE 5. (**a**) Average <Ca-O > (solid diamonds) and <Ti-O> (crosses) bond length as a function of cell volume. Only <Ca-O> shows a significant correlation. Its range is relatively small due to the opposite behavior of Ca-O bonds parallel and perpendicular to the a-axis, respectively. For the <Ti-O> bonds, no correlation within the limits of the standard deviations is found. (**b**) Average <Si-O> bond lengths as a function of temperature. There is only a weak negative correlation to be recognized. Note that during the initial stages of the Rietveld refinements, the Si-O bonds were soft constrained to 1.63 Å.

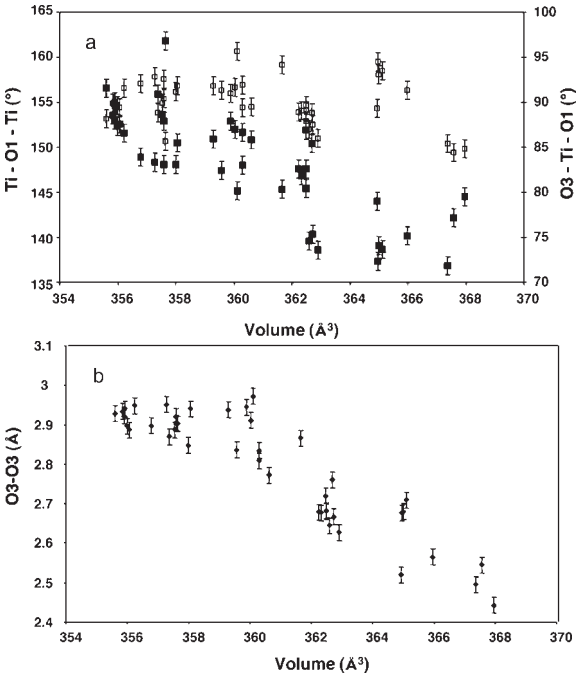

FIGURE 6. (**a**) Variation of the Ti-O1-Ti (solid squares) and O3-Ti-O1 (open squares) angle (see Fig. 7) with changing cell volume. The significant negative correlation of the Ti-O1-Ti indicates a straightening of the TiO_6 chains with decreasing volume. The only small scatter around 90° for the O3-Ti-O1 angle and the lack of any correlation indicate a rigid behavior of the TiO_6 octahedra without any significant intra-octahedral distortion. (**b**) Change of the O3-O3 distance with varying volume. The increase in O3-O3 distance with decreasing volume indicates a straightening of the TiO_6 chain with decreasing volume and vice versa.

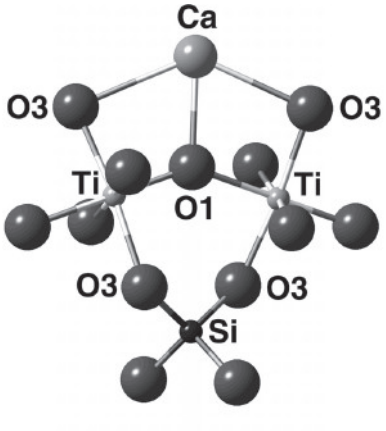

FIGURE 7. Ball-and-stick model of a part of the titanite structure illustrating the structural angles and bonds, discussed in the text.

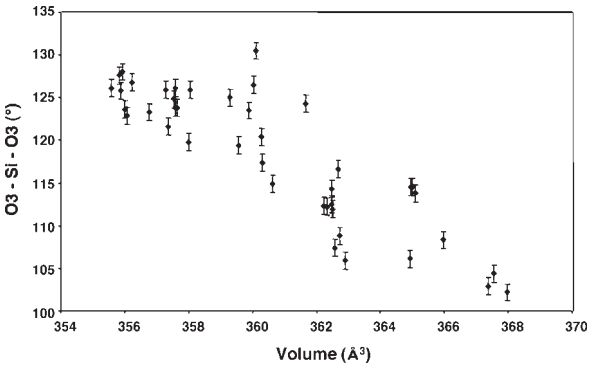

FIGURE 8. Variation of the intra-tetrahedral O3-Si-O3 angle with changing volume. There is strong negative correlation demonstrating that the rigid rotation of the TiO_6 octahedra is compensated by a tetrahedral angular distortion.

rigid unit modes are highly unlikely in titanite. This is mainly due to the topology of corner-linked octahedra and tetrahedra hampering polyhedral rotations. However, an increase of the O3-O3 oxygen distance (Fig. 8) implies at least an opening of the O3-Si-O3 angle if not an increase of the Si-O3 bond distance. This suggests the paradoxical situation of a potentially increasing Si-O bond length with decreasing unit-cell volume as caused for example by increasing pressure. Whereas we observe a (within uncertainties) constant Si-O bond distance as a function of pressure, the variation of the O3-Si-O3 angle with volume is systematic and significant with a maximal tetrahedral angle of around 130° at minimal volume (Fig. 8). The distortion of the O3-Si-O3 angle thus enables the quasi-rigid rotation of the Ti-octahedra. A similar rigid octahedral rotation has previously been observed in malayaite (Bismayer et al. 1999) and, on the basis of the toplogical identity of the structures, was also postulated for titanite, and confirmed here.

The negative correlation between volume and Ti-O1-Ti angle can now be addressed. Due to the overall positive correlation between the *a*-axis and volume, the stretching of the Ti-octahedral chain has to be accompanied by a shortening of the *a*-axis to which the chains are parallel. This means that the opening of the Ti-O1-Ti angle has to be overcompensated by a corresponding shortening of the average <Ti-O1> bonds and vice versa. We assume the driving force behind the stretching of the octahedral chains to be the compression of the Ca polyhedra. As suggested by Kunz et al. (1996) and Angel et al. (1999a), it is the soft CaO_7 polyhedra, which dominate the compression behavior of titanite. The Ca atoms share among others two O3-O1 edges with the TiO_6 octahedra (Fig. 7). The Ca-O3 bonds to the shared edges are relatively long (~2.6–2.7 Å) and are thus very effectively compressed in terms of energy needed for a given shortening. A compression of the Ca-O3 bond thus pulls the two O3 oxygen atoms together and by this way straightens the octahedral chains in the absence of any intra-octahedral distortions. This also should lead to a lengthening of the Ca-O1 bond with decreasing volume, as observed. In summary, the long bond lengths of the soft CaO_7 polyhedron are easiest to accommodate any temperature or pressure driven volume change even on the cost of a negative correlation of Ca-O1 with cell volume. The TiO_6-SiO_4 polyhedral framework adjusts by rigid rotations of the TiO_6 octahedra together with a twisting of O3-Si-O3 angles and possibly even lengthening of the <Si-O> bonds.

ACKNOWLEDGMENTS

This work benefited greatly from discussions with Ross Angel, BGI, Bayreuth. Constructive comments of Ulrich Bismayer improved this publication significantly. Beamline assistance on ID30 of Mohammed Mezouar and Tristan LeBihan is acknowledged. We thank François Guyot (Université Paris 7) for lending us the heatable diamond anvil cell. Isabelle Daniel and Guillaume Fiquet (ENS Lyon) were extremely helpful with instructions on the handling of this particular DAC. This project is supported by the Schweizerischer Nationalfonds grant no. 20-52682.97 to Martin Kunz.

REFERENCES CITED

Angel, R.J. (2000) Equations of State. In B. Hazen, Ed., Comparative Crystal Chemistry, in press. Reviews in Mineralogy and Geochemistry, Mineralogical Society of America and The Geochemical Society, Washington, D.C.

Angel, R.J., Kunz, M., Miletich, R., Woodland, A.B., Koch R., and Xirouchakis D. (1999a) High-pressure phase transition in $CaTiOSiO_4$ titanite. Phase Transitions, 68, 533–543.

Angel, R.J., Kunz, M., Miletich, R., Woodland, A.B., Koch, M., and Knoche, R.L. (1999b). Effect of isovalent Si, Ti substitution on the bulk moduli of $Ca(Ti_{1-x}Si_x)SiO_5$ titanites. American Mineralogist, 84, 282–287.

Bismayer, U., Schmahl, W., Schmidt, C., and Groat L.A. (1992) Linear Birefringence and X-ray Diffraction Studies of the Structural Phase Transition in Titanite, $CaTiSiO_5$. Physics and Chemistry of minerals, 19, 260–266.

Bismayer, U., Zhang, M., Groat, L.A., Salje, E.K.H., and Meyer H-K. (1999) The beta-gamma phase transition in titanite and the isosymmetric analogue in malayaite. Phase Transitions, 68, 545-556.

Birch, F. (1947) Finite elastic strain of cubic crystals. Physical Review, 71, 809–824.

Carpenter, M.A. and Salje, E.K.H. (1998) Elastic anomalies in minerals due to structural phase transitions. European Journal of Mineralogy, 10, 693–812.

Chrosch, J., Bismayer, U., and Salje, E.K.H. (1997) Anti-phase boundaries and phase transitions in titanite: An X-ray diffraction study. American Mineralogist, 82, 677–681.

Fei, Y.W., Mao, H.K., Shu, J.F., Parthasarathy, G., Bassett, W.A., and Ko, J.D. (1992) Simultaneous high-P, high-T X-ray-diffraction study of beta-$(Mg,Fe)_2SiO_4$ to 26 GPa and 900 K. Journal of Geophysical Research-Solid Earth, 97, (B4) 4489–4495.

Fiquet G., Andrault, D., Dewaele, A., Charpin, T., Kunz, M., and Häusermann, D. (1998) *P-V-T* equation of state of $MgSiO_3$ perovskite. Physics of the Earth and Planetary Interiors, 105, 21–31.

Hammersley, A.P. (1997) FIT2D: An introduction and overview. ESRF Internal

Report ESRF97HA02T.
Hammersley, A.P., Svensson, S.O., Thompson, A., Graafsma, H., Kvick, Å., and Moy, J.P. (1995) Calibration and correction of distortions in 2D detector systems. Review of Scientific Instruments, 66, 2729–2733.
Hammersley, A.P., Svensson, S.O., Hanfland, M., Fitch, A.N., and Häusermann, D. (1996) Two-dimensional detector software: From real detector to idealised image or two-theta scan. High Pressure Research, 14, 235–248.
Hammonds, K.D., Bosenick, A., Dove, M.T., and Heine, V. (1998) Rigid unit modes in crystal structures with octahedrally coordinated atoms. American Mineralogist, 83, 476–479.
Hayward, S.A., del Cerro, J., and Salje, E.K.H. (2000) Antiferroelectric phase transition in titanite: Excess entropy and short range order. American Mineralogist, 85, 557–562.
Kek, S., Aroyo, M., Bismayer, U., Schmidt, C., Eichhorn, K., and Krane, H.G. (1997) The two-step phase transition of titanite, $CaTiSiO_5$: A synchrotron radiation study. Zeitschrift für Kristallographie, 212, 9–19.
Kunz, M. and Brown, I.D. (1994) Out-of-center distortions around octahedrally coordinated d^0-transition metals. Journal of Solid State Chemistry, 115, 395–406.
Kunz, M., Dinnebier, R., Cheng, L.K., McCarron, E.M., Cox, D.E., Parise, J.B., Gehrke, M., Calabrese, J., Stephens, P.W., Vogt, T., and Papoular, R. (1995) Cs(TiAs)O5 and $Cs(TiP)O_5$: A disordered parent structure of $ABOCO_4$ compounds. Journal of Solid State Chemistry, 120, 299–310.
Kunz, M., Xirouchakis, D., Lindsley, D.H., and Häusermann, D. (1996) High-pressure phase transition in titanite ($CaTiOSiO_4$). American Mineralogist, 81, 1527–1530.
Kunz, M. Xirouchakis, D., Yanbin, W., Parise J.B., and Lindsley, D.H. (1997) Structural investigations along the join $CaTiOSiO_4$-$CaSnOSiO_4$. Schweizerische Mineralogische Petrographische Mitteilungen, 77, 1–11.
Larson, A.C. and Von Dreele R.B. (1994) GSAS, General Structure Analysis System, Manual, Los Alamos National Laboratory, LAUR 86–748.
Le Bail, A. (1992) Extracting structure factors from powder diffraction data by iterative full pattern profile fitting. In E. Prince and J.K. Staijek, Eds., Accuracy in Powder Diffraction II, Special Publication 846,213. National Institute of Standards and Technology, Gaithersburg, Maryland.
Martinez, I., Wang, Y., Liebermann, R.C., and Guyot, F. (1997) Microstructures and iron partitioning in $(Mg,Fe)SiO_3$-perovskite (Mg,Fe)O-magnesiowüstite assemblages: An analytical transmission electron microscopy study. Journal of Geophysical Research, 102, (B3) 5265–5280.
Oberti, R., Smith, D.C., Rossi, G., and Caucia, F. (1991) The crystal chemistry of high-aluminum titanites. European Journal of Mineralogy, 3, 777–792.
Saxena, S.K. and Zhang, J. (1990) Thermochemical and pressure-volume-temperature systematics of data on solids, example: tungsten and MgO. Physics and Chemistry of Minerals, 17, 45–51.
Tangeman, J.A. and Xirouchakis, D. (2000) High temperature heat capacity and thermodynamic properties of end-member Titanite. Physics and Chemistry of Minerals, in press.
Taylor, M. and Brown G.E. (1976) High-temperature structural study of the $P2_1/a \leftrightarrow A2/a$ phase transition in synthetic titanite, $CaTiSiO_5$. American Mineralogist, 61, 435–447.
Thoms, M., Bauchau, S., Häusermann, D., Kunz, M., LeBihan, T., Mezouar, M., and Strawbridge D. (1998) An improved X-ray detector for the use at synchrotrons. Nuclear Instrumentation and Methods in Physics Research, A 413, 175–184.
Xirouchakis, D., Kunz, M., Parise J.B., and Lindsley, D.H. (1997) Synthesis methods and unit cell volume of end member titanite ($CaTiOSiO_4$) American Mineralogist, 82, 748–754.
Zhang, M., Salje, E., Bismayer, U., Unruh, H., Wruck, B., and Schmidt, C. (1995) Phase transition(s) in titanite ($CaTiSiO_5$) An infrared spectroscopic, dielectric response and heat capacity study. Physics and Chemistry of Minerals, 22, 41–49.

MANUSCRIPT RECEIVED FEBRUARY 23, 2000
MANUSCRIPT ACCEPTED MAY 19, 2000
PAPER HANDLED BY YANBIN WANG